SLAC-PUB-9557
October 2002

RADIATION PROTECTION AT HIGH-ENERGY ELECTRON ACCELERATORS

Vaclav Vylet [1] and James C. Liu [2]

1. OESO/DUMC Box 3155, Duke University, Durham, NC 27710, USA
2. Stanford Linear Accelerator Center, P. O. Box 20450, Stanford, CA 94309, USA

Abstract
This work presents an overview of radiation protection at high-energy electron accelerator facilities. By "high-energy" we mean the energy domain beyond few tens of MeV, where electromagnetic showers are the determining and dominant factor in beam interactions with matter. We describe basic components of electron accelerators and their potential impact on radiation safety. We then concentrate mainly on sources of prompt radiation which distinguish these machines from other accelerator facilities. In other areas we only mention details relevant to electron machines. More comprehensive description of these aspects, such as shielding or safety systems, can be found elsewhere in this issue. General concepts presented in this review are complemented and illustrated by more specific examples in our follow-up work in this issue(1).

*Work supported by Department of Energy contract DE-AC-03-76SF00515

Invited Talk Presented at 10th Course on Accelerator Radiation Protection,
International School of Radiation Protection and Damage, 10/2/2001-10/9/2001, Erice, Italy

ANATOMY OF AN ELECTRON ACCELERATOR

High-energy electron accelerators are complex devices containing many components. Linacs and synchrotron rings are two very common configurations, but other configurations are possible. For example, CEBAF at the Thomas Jefferson Lab uses two linacs connected by two five-fold "racetrack" arcs to recirculate the electron beam. Regardless of the configuration, all facilities contain the same basic systems: accelerator structures and associated RF power equipment, hardware associated with steering and focusing the beam, vacuum systems, alignment, water cooling, AC power, diagnostic instrumentation and control systems, personnel protection systems and shielding. Most of these components may have direct or indirect impact on radiation safety. As an example, we will illustrate a few important components of an electron linac shown in Figure 1. The specific configuration chosen here is simplified for illustration purposes and may not represent the best choice from accelerator physics point of view. A more detailed discussion of individual components is included below.

Klystrons provide RF power used to accelerate electrons in accelerator cavities. RF waves are excited in the klystron cavity by the passage of electron bunches. These electrons are accelerated to energies on the order of a few hundred keV and terminate their path in the klystron collector, generating copious amounts of X-rays. Because klystrons are usually situated outside the accelerator enclosure, it is important to ensure that their shielding is adequate. Aging klystrons may generate X-rays in other locations besides collector, requiring additional local shielding. Frequent surveys of klystrons are therefore recommended.

Electron Gun is the initial source of electrons. *Thermionic* guns use a heated cathode to reduce the work function of electron emission. Electrons are extracted either by DC high voltage (DC HV guns) or by RF power (RF guns). The latter allow much higher field gradients and resulting electron energies. In *photocathode* guns, electrons in the cathode material are excited by a laser pulse, with minimal thermal heating of the cathode. They may be used with either DC or RF extraction mode. Acceleration stages following the gun have specific requirement on electron bunch structure and frequency. Consequently, a large portion of the current generated by the gun may not be accepted and will be lost at the gun exit or in the first portion of the accelerator. The gun area may therefore be an intense source of radiation, albeit of low energy. In general, this problem is more acute in thermionic guns. For example, in a thermionic RF gun the pulse structure is determined by the frequency of the rf structure and the beam has a large energy spread[(2)]. An alpha magnet is typically required to reduce the energy spread of the beam and a chopper may be used to select bunches with acceptable timing. Both these devices will be sources of radiation. Photocathode RF guns generate much shorter pulses and pulse structure is determined by the laser pulse structure, which can be better matched to the acceptance of following accelerator stages. While use of photocathode RF guns usually leads to lower beam losses at the injection and later acceleration stages, at very high RF gradients the gun may exhibit the so-called "supercharged" mode. In this case, a few remnant electrons are accelerated into the cathode by the oscillating RF field and knock out other electrons. As a result, the gun keeps producing electrons by RF

excitation, long after the laser pulse ended. This may increase the gun output by a factor of ~100[3] and the maximum allowed beam power may be exceeded.

Dipole magnets, also called *bending magnets*, are used to steer the beam into a desired direction. Relatively weak corrector dipole magnet**s** are used to adjust the beam trajectory in a linac. They are usually used in pairs, one for horizontal and another for vertical direction. Stronger dipoles are required in storage rings or linac chicanes. A chicane is an arrangement where the beam is bent out of line and then brought back by a series of dipoles, with the purpose of selecting electrons in a narrow momentum range. An example of a chicane is illustrated in the first third of the linac in Figure 1.

The energy of the electron beam at the end of the acceleration stage may be determined by use of spectrometer dipole magnets. High energies at this point require use of high magnetic fields and spectrometer magnets may be very massive. By their nature, dipole magnets may steer the beam into undesirable directions under various failure scenarios. This possibility needs to be considered in radiation safety analysis. Local shielding or collimators may be used to mitigate effects of such failures.

A special sort of beam bending devices are pulsed or *kicker magnets* and *septa*. These devices are usually used at switching points in beam lines, *e.g.* when the beam is injected from one accelerator to another. Substantial beam losses, and consequently radiation fields, usually occur in the vicinity of these devices.

Quadrupole magnets are used to focus the electron beam. Improper adjustment may cause beam losses by overly spreading the beam, and the fringe area of a quadrupole field acts as a dipole. Sextupole and octupole magnets are also used for higher degree corrections in beam optics. In general, all magnets are potential points of beam mis-steering. On the other hand, tightly packed arrays of magnets may attenuate effects of beam loss in a beam pipe wall and prevent shower development in the shielding wall. When hit by a beam, they usually constitute a “thick” target.

Beam diagnostic covers a number of different devices that can either generate radiation when hit by beam and/or be used as part of safety systems. One such device is *Average Current Monitor* (ACM) consisting of a toroid mounted over the beam pipe. Their signal is proportional to beam current. A couple of ACMs may be used as Current Comparator, *i.e.* device indicating the magnitude of beam loss in the beam line between the two ACMs. Other diagnostic devices make use of screens or wires that can be inserted into the beam. Such devices usually measure beam shape and profile of the beam spot, either using a video camera or other measurement techniques. Beam losses caused by these devices may generate undesirable levels of radiation and may require local shielding. An insertable *Faraday cup* (FC) is a device massive enough to completely stop the beam and measure the accumulating charge. It can be used both as diagnostic device and a safety stopper. Again, it is a source of radiation and may require local shielding. Beam dumps, where the beam is terminated, are often also used as a diagnostic device (FC). Diagnostic devices, and sometimes dipole magnets as well, may be interlocked as part of a radiation safety system. Details of such configurations are described by Liu et al[4] elsewhere in this issue. In this paper the reader will also find

information about additional safety devices, such as burn-through monitors and radiation monitors, used both in machine and personnel protection systems.

Accelerator sections are copper cavities accelerating electrons by means of standing or traveling RF wave. A certain amount of distributed beam loss occurs in the sections, usually more so in the early acceleration stages. Before or jus after installation, a new accelerator section needs to undergo *RF processing*, *i.e.* being gradually subjected to increasing amounts of RF power, to "burn out" surface impurities and imperfections. No beam is injected during this procedure, but the section generates strong dark current and may be subject to arcing. This procedure is likely to generate great amounts of X-rays and requires adequate radiation protection measures.

Experimental equipment is routinely inserted in beam path to conduct scientific experiments – this may be the main goal of operating a given accelerator. It may be a simple target or a complex setup of targets and detectors. Secondary radiation may be generated in such devices

Cooling system usually consists of a closed circuit of de-ionized water, which helps to limit water activation. It is used to dissipate heat from devices exposed to high beam power, such as beam dumps, stoppers, collimators or synchrotron heat shields. Components not directly exposed to beam, such as magnets, may also require cooling. When a device is not capable to withstand allowed beam power without cooling, flow-switch interlocks are usually required by machine (and possibly personnel) safety system. As indicated above, this cooling water is activated. The cooling circuit is therefore a source of radiation and requires adequate radiation protection measures. Dealing with leaks and proper waste water disposal need also be considered.

Vacuum system consists of vacuum pumps connected to sections of beam pipe and some experimental devices crossed by the beam path. A good vacuum minimizes beam losses on residual air and generation of gas bremsstrahlung (see more details in reference (1)). Automatic valves isolate separate section of the system and enter in action if the vacuum deteriorates in a given area. If in such instance the machine protection system does not stop the beam, the beam can hit the valve and generate radiation. For the purpose of source term estimation, a typical valve can be considered as a thin target.

PROMT RADIATION SOURCES

Prompt radiation fields are generated by beam loss in beam line components and other material that may be hit by the beam. Partial or total beam loss is expected in or around components such as injection lines, collimators, slits, beam stoppers and beam dumps. Unplanned beam losses result from beam mis-steering due to inaccurate orbit adjustment or equipment failure. At electron energies considered here electrons striking a target material will interact by developing an *electromagnetic (EM) cascade* or *shower*, and the secondary particles generated in the cascade result in a prompt radiation field. Radiation

fields of concern behind shielding of high-energy electron accelerators consist mainly of photon and neutrons. At very high energies, starting around 1 GeV and higher, muons are also of concern in a narrow forward area along the axis of the beam, *i.e.* at 0º behind beam dumps. Source terms for these components are presented in Figure 2 in terms of dose-equivalent rate per unit beam power. In the following text we will present a closer look at EM cascades and the different components of the prompt radiation field.

Development of EM cascade

Critical energy E_c for a given material defines the boundary where electron collision losses equal radiation losses. A good estimate of E_c can be obtained from the well known expression, E_c [MeV] = 800/(Z + 1.2). Beam energies at high-energy electron accelerators are well above E_c for common materials used in beam lines. As a result, high-energy electrons hitting target material will loose energy almost exclusively by generating bremsstrahlung photons. An electron (with $E >> E_c$) generates a photon after traversing on average a distance X_0 [g/cm^2], called *radiation length*, and loosing (by definition of X_0) (1-1/e) ≈ 0.63 of its initial energy. Such high-energy photon will most likely interact by pair production, as can be expected from photon cross-sections illustrated in Figure 3. This photon will produce an electron-positron pair after traveling a distance of 9/7X_0 on average. Both the positron and electron will generate bremsstrahlung photons, again after an average distance of X_0, continuing the multiplication process, hence the term cascade. The number of the particles in the cascade roughly doubles at each step as described above, until the energy of electrons falls below E_c. Beyond this point electron energy loss is progressively dominated by Compton scattering, other collision processes and photoelectric absorption. An example of electromagnetic shower initiated by a single 1 GeV electron in copper target is shown in Figure 4.

Obviously, EM cascades can be also initiated by high energy photons. It follows from the above that EM cascades in different materials can be conveniently described using X_0 and E_c as scaling parameters, *i.e.* describing distance x as $t = x/X_0$ in units of radiation length, and energy E as $y = E/E_c$ in units of critical energy. The following relationships approximately describe shower behavior[5]:

Energy deposition profile:
$$\frac{dE}{dt} = E_0 b \frac{(bt)^{a-1} e^{-bt}}{\Gamma(a)} \qquad (1)$$

where E_0 is the initial electron energy. Values of b are tabulated for different materials; in most cases b=0.5 is adequate. Value of a then can be determined using equation (2) below.

Shower maximum, *i.e.* the maximum of the energy deposition profile above, occurs at a depth of

$$t_{\max} = \frac{a-1}{b} = 1.0 \times \left(\ln y + C_j\right) \qquad j = e, \gamma \qquad (2)$$

where C_e = -0.5 for electron-induced cascades, and C_γ = +0.5 for photon-induced cascades.

The radial shower distribution is usually described in terms of Molière radius X_m:

$$X_m = \frac{X_0 E_S}{E_c} \qquad (3)$$

where E_S = 21.2 MeV. Approximately 90% of energy deposited by the shower is included within a radius r = 1 X_m, and this fraction becomes 99% for r = 3.5 X_m.

Bremsstrahlung

Prompt photon fields produced by bremsstrahlung constitute the most important radiation hazard from electron machines with thin or no shielding. Bremsstrahlung yield is very forward peaked, and increasingly so with increasing energy. This behavior is described by the following equation:

$$\theta_{1/2} = 100 / E_0 \qquad (4)$$

where $\theta_{1/2}$ is in the angle in degrees at which the intensity drops to one half of that at 0º, and E_0 is the energy of the initial electrons in MeV. In the context of bremsstrahlung, a "thick target" usually means a target of sufficient thickness to maximize bremsstrahlung production, so that increasing the thickness beyond this point would lead to lower yield, due to photon attenuation in the target. Photon yield from a thick target as a function of angle consists of two components: sharply varying forward component, described in equation (4), and a mildly varying wide-angle component. Forward (or zero-degree) bremsstrahlung contains the most energetic and penetrating photons, while bremsstrahlung at wide angles is much softer. These two components are illustrated in Figure 5 in terms of photon dose equivalent rate per unit beam power, as implemented in the analytical model used by the shielding code SHIELD11[10] discussed further below. It is apparent from the analytical expressions in Figure 5 (see also equation 9 below), that while the forward bremsstrahlung component is proportional to electron energy, the wide angle component scales only with beam power. This behavior is captured in "rules of thumb" by Swanson[5] for thick-target bremsstrahlung at 0º and 90º, again expressed in terms of photon dose rate per unit beam power:

$$\dot{D}\left[\mathrm{Gy.h^{-1}.kW^{-1}.m^{2}}\right] \approx 300 E_0 \qquad \text{at } 0^\circ,\ E_0 > 20 \text{ MeV} \qquad (5)$$

$$\dot{D}\left[\mathrm{Gy.h^{-1}.kW^{-1}.m^{2}}\right] \approx 50 \qquad \text{at } 90^\circ,\ E_0 > 100 \text{ MeV} \qquad (6)$$

Equations (5) and (6) express approximations for "high-Z" targets. Variation of these source terms with Z is a mild one and can be neglected in first approximation for radiation protection purposes. Mao et al.[11] calculated bremsstrahlung spectra from thick targets at 90º for electron energies from 50 MeV to 10 GeV and concluded that

- shapes of these spectra are independent of the incident electron energy,
- 99.9% of photons at 90º have energies below 10 MeV,

- most photons with energies below 1.5 MeV are produced by Compton scattering, and
- photons with energies between 1.5 and 10 MeV are mostly produced by small-angle bremsstrahlung emitted by secondary electrons traveling at large angles due to multiple scattering.

These results confirm that the source term (per unit beam power) for bremsstrahlung at 90º is independent of energy, as inferred by Figure 2 and Equation (6). An example of spectra at 90º from a thick copper target is presented in Figure 6.

Even when the electron beam is perfectly steered, without hitting solid obstacles, it still interacts with atoms of residual gas in the evacuated beam pipe, generating the so-called *gas bremsstrahlung*. Yield of gas bremsstrahlung per unit beam current is proportional to both the length of the straight beam path through the gas column and the gas pressure. Virtual absence of multiple scattering contributes to the fact that yield of gas bremsstrahlung is extremely forward-peaked, more so than from thick solid targets. Because this source of prompt radiation is of interest mainly at synchrotron light and free electron laser facilities, it is addressed in more detail in a follow-up article[(1)] devoted to this subject.

Neutrons.

Because photons have substantially larger nuclear cross-sections than electrons, neutrons and other particles resulting from inelastic nuclear reactions are produced mainly by the photon component of the EM shower. It is evident from Figure 3 that these photo-nuclear processes have little importance in the development and attenuation of EM showers. Neutrons from photonuclear reactions are outnumbered by orders of magnitude by electrons and photons that form the cascade. However, some of these neutrons constitute the most penetrating component (except the special case of muons – see below) of the prompt radiation field, and will therefore be determining factor for radiation fields behind thick shielding. Three photoneutron production processes are important at high-energy electron facilities, as illustrated in Figure 3.

Giant Resonance Production. This process can be seen in two steps: excitation of the nucleus by photon absorption, and subsequent de-excitation by neutron emission, where memory of the original photon direction has been lost. As a result, the angular yield of giant resonance neutrons is nearly isotropic. The cross-section has large maximum around 20-23 MeV for light nuclei (mass number $A \leq 40$) and 13-18 MeV for heavier nuclei. For $A \geq 40$ the energy of the cross-section peak is approximately given by $k_0 = 80.A^{-1/3}$ MeV[(5)]. In order to estimate the neutron yield, this cross-section has to be folded with the photon spectrum in the target. For thick targets, shapes of these spectra are assumed to vary as $\sim 1/k^2$, where k is photon energy. The integrated giant resonance cross-section over the relevant energy interval of 0 to 30 MeV, weighted by a $1/k^2$ spectrum, is σ_{-2} and it varies as $\sim A^{5/3}$ [(5)]. For thin targets the bremsstrahlung spectrum is $1/k$. Similarly, one can obtain an integrated cross-section $\sigma_{-1} \sim A^{-4/3}$. Neutron spectra from this process consist of “evaporation” and “direct emission” neutrons, where the

former component is the dominant one. Evaporation spectra can be described by a Maxwellian distribution, with nuclear temperatures typically between 0.5 and 1.0 MeV. It is clear from the size of the giant resonance cross-section and the higher weight of low-energy photons in bremsstrahlung spectra that this is the dominant process of photoneutron production at electron accelerators at any electron energy.

Pseudo-deuteron production. At photon energies beyond the giant resonance, the photon is more likely to interact with a neutron-proton pair rather than with all nucleons collectively. This mechanism is important in the energy interval of 30 to ~300 MeV, contributing to the high-energy end of the giant resonance spectrum. Because the cross-section is an order of magnitude lower than giant resonance, with the added weighting of bremsstrahlung spectra, this process never dominates. In its more heavily weighted portion below 125 MeV, the cross-section varies as 1/*k*. Spectra of pseudo-deuteron neutrons can be approximately described by

$$\frac{dN}{dE_n} \approx E_n^{-\alpha} \qquad \text{for 5 MeV} < E_n < E_0/2 \qquad (7)$$

where *a* varies from 1.7 to ~3.6, with values increasing from lighter to heavier nuclei.

Photo-pion production. Above the threshold of ~140 MeV production of pions (and other particles) becomes energetically possible. These pions then generate secondary neutrons as byproduct of their interactions with nuclei. The cross section (labeled 3 in Figure 3) exhibits several resonances, the first occurring around 300 MeV. In the GeV region and beyond, the photonuclear cross-section is approximately constant. Due to the energy weighting by bremsstrahlung spectra, the most high-energy neutrons will be produced by the first resonance at 300 MeV. While substantially less numerous than giant resonance neutrons, the photopion neutrons are very penetrating and will be the component of the initial radiation field from a target (with the exception of muons at very high energies) that determines the radiation fields outside very thick shields. This high-energy component generates along its path through shielding a following of secondary neutrons and photons, resulting from processes such as spallation, evaporation and capture. Beyond a certain shielding thickness an equilibrium is established between the generating high energy neutrons and the associated lower-energy neutrons, forming together a so-called equilibrium spectrum. Equilibrium spectra emerging from outer shielding layers at high energy proton and electron machines are very similar, because in both cases they are “fueled” by the most penetrating high-energy neutron component, and memory of the original mechanism and composition has been erased.

Skyshine. Roofs of accelerator enclosures are typically thinner than the side shielding walls. A few electron facilities are not shielded at all in the vertical direction. Neutrons streaming upwards and scattering in the air can reach areas on the ground at large distances from the accelerator facility. This so-called neutron “skyshine” is the prompt radiation field component, which is usually the most relevant for radiation exposures at

site boundary and in public areas beyond. Its variation with distance r can be adequately described in simple terms[12]:

$$\Phi(r) = \frac{Q.e^{-r/\lambda}}{r^2} \qquad (8)$$

where $\Phi(r)$ is neutron fluence rate, Q is neutron emission from the surface and λ is an effective absorption length for neutrons in air. This value will depend on the neutron energy spectrum, values from $\lambda < 300$ m to $\lambda > 1000$ m have been reported. Liu *et al*[13] performed measurements of skyshine at SLAC under stable conditions from a 2.3 GeV electron beam on a thick target. Regression of the results by a functional form from equation (8) yields $\lambda \approx 500$ m. These measurement results are illustrated in Figure 7, in comparison with results of the SKYSHINE[14] code described further below. It should be noted that some authors found a better fit to experimental data at their facilities when the $1/r^2$ term in equation (8) is replaced by $1/r$. Based on theoretical considerations, Lindenbaum[15] developed a formula with both $1/r^2$ and $1/r$ additive terms, where the former dominates at shorter distances and the latter at larger ones. It is probably true that data limited to a certain distance range at a given facility may be successfully fitted with either model[16]. In this case a fit using equation (8) requires larger λ values than in case of $1/r$ behavior. In comparison with the value of $\lambda \approx 500$ m above, Jenkins[16] found $\lambda \approx$ 140 m from his measurements at SLAC, using the $1/r$ dependency.

Muons

Muon production is analogous to e^+/e^- pair production by photons in the field of target nuclei when photon energy exceeds the threshold $2m_\mu c^2 \approx 211$ MeV. Compared to pair production, μ^+/μ^- pair will occur with a much lower probability. Because the pair production cross-section is inversely proportional to the square of rest mass, muon pair production is $(m_\mu/m_e)^2 \approx 4.10^4$ less likely than electron pair production. Similarly, due to their large mass, muons (unless at extremely high energies) do not lose energy by bremsstrahlung. Because they are leptons and do not initiate nuclear reactions, they dissipate their energy essentially by ionization. Crude estimates can be done assuming that this energy loss happens at a "minimum ionizing" rate of ~2 MeV g^{-1} cm^2. Above a few GeV the muon yield per unit electron beam power is approximately proportional to electron energy E_0. Muon angular distribution is extremely forward-peaked, and this distribution narrows further with increasing energy. For beam energies below ~1 GeV, adequate photon and neutron shielding will be also sufficient for muons. Muons generally become a problem at higher energies mainly behind beam dumps, and only within a narrow cone of a few degrees, depending on energy, around the 0º direction. A source term for muon from a thick target, expressed as dose equivalent rate per unit electron beam power, is presented in Figure 8.

Synchrotron radiation

Charged particles on a curved path, such as one through a dipole magnet, emit radiation of relatively low energies, called *synchroton radiation*. Because the yield for a given particle species depends on its mass as m^{-4}, it is clear that this phenomenon is of substantially higher interest at electron machines. In conventional electron accelerators

synchrotron radiation is seen mainly as a source of undesirable heat deposition in beam lines near bending magnets, although it has beneficial effects of energy and bunch length damping[2] in ring electron accelerators. Widespread use synchrotron radiation in various areas of scientific research spurred the growth of high-energy electron facilities built specifically for this purpose. More on these facilities and synchrotron radiation can be found in another article[1] in this compendium.

INDUCED ACTIVITY

General aspects of radioactivity induced in components, air and water at particle accelerators are well covered in this compendium by G. Stevenson[18]. We will briefly mention here only a few aspects specific to high-energy electron machines.

Although an important aspect of radiation protection, induced activity at electron accelerators is of lesser concern than at proton machines. Figure 2 indicates the range of source terms expected from activated components and puts it in perspective with those from prompt radiation sources. The three photonuclear reactions described in the previous section are responsible for most of the produced activity in the machine components. Furthermore, neutrons resulting from these reactions can activate surrounding materials (*e.g.* soil and air).

Estimates of induced activity in beam line components can be made from data available in literature expressed in terms of saturated activity A_s per unit electron beam power. Extensive listing A_s values, and corresponding exposure rate values, for different materials has been compiled by Swanson[5]. Effects of self-shielding and activity distribution depend on local geometry and are therefore not included in A_s. These effects can be estimated under some simplifying assumptions as shown by DeStaebler[19].

According to their susceptibility to activation around high energy electron machines, Swanson[5] classifies various materials in following categories:

- Low: lead, ordinary concrete, aluminum, wood, plastics
- Moderate: iron (steel, ferrites), copper
- High: stainless steel, tungsten, tantalum, zinc, gold, manganese, cobalt, nickel
- Fissionable: uranium, plutonium, thorium

Swanson lists also A_s values for air activation, in this case per unit path length of bremsstrahlung through air. Estimates therefore require knowledge of this quantity, which can be estimated in case of simple geometries. In more complex cases Monte-Carlo calculations are preferable. While important activation products, ^{11}C, ^{13}N, ^{15}O, are directly produced by photonuclear reactions in air, ^{41}A is produced by thermal neutron capture. Its concentration can be estimated from the knowledge of the macroscopic cross-section for capture and fluence rate of thermal neutrons, generated by slowing down of fast neutrons in the concrete shielding of the accelerator enclosure. The latter can be estimated using Patterson's formula: $\Phi_{th} \approx 1.25 \times Q/S$, where Q is the source strength of fast neutrons and S is the surface over which they are thermalized[20].

An excellent overview of methods used to predict induced activity specifically at high-energy electron machines, including new advances in application of Monte Carlo simulations in this area, can be found in a recent work by Fassò *et al*[21]. Rokni *at al*[22] recently irradiated a number of materials in stray fields from a 28.5 GeV electron beam and compared their experimental results with calculations using the FLUKA[23] Monte-Carlo code.

SHIELDING

General aspects of accelerator shielding are described in detail by Stevenson[24], and specific aspects, such as labyrinths and ducting, are also developed in other papers[25,26] in this compendium. From the discussion of components of the prompt radiation fields the following conclusions generally apply to high-energy electron accelerators:

- Photons and giant resonance neutrons dominate the field inside shielding enclosures and remain a significant component behind moderate shielding. For example, a 60 cm lateral concrete shielding of a 3 GeV electron beam line with average beam power of 5 W can be considered as moderate.
- High-energy neutrons, and associated evaporation neutrons and photons generated in the shield, are the determining factor for design of thick shielding.
- For neutrons with energies above ~20 MeV the best shielding configuration consists of a layer of high-*Z* material, such as lead or steel, followed by a low-*Z* shield with high hydrogen content – most often concrete. This scheme takes advantage of high inelastic cross sections in high-*Z* materials to reduce the neutron energy by *(n,xn)* and other inelastic processes. The lower energy neutrons generated in this process are then best attenuated and moderated in hydrogenous material to thermal energies. The first high-*Z* layer is also efficient for shielding photons of all energies.
- It is best to design beam lines so that EM showers from occasional mis-steering or planned losses are fully contained in potential targets or additional collimators, so that no further shower development is allowed to occur in concrete shielding walls. Due the distance factor and large physical size of a shower in concrete (large X_0), it could result in extremely high radiation levels in occupied areas.
- At high energies additional high-*Z* shielding in the forward direction behind beam dumps may be required. At very high energies completely ranging out muons may be impractical. Muon dose rates can be controlled by using partial shielding for fluence reduction due multiple scatter and taking advantage of distance, with possible use of narrow exclusion zones around the 0º direction.

There is a general consensus that Monte-Carlo codes, such as FLUKA, EGS4, MCNPX[27] or MARS[28], will provide the most accurate results for shielding design purposes, in particular for complicated three-dimensional geometries. However, when conditions allow, a lot of time and effort can be spared by use of simpler methods. In the following section we would like to mention some simple shield design codes useful to

practitioners specifically at high-energy electron facilities. These codes make use of semi-empirical models for radiation source terms and attenuation through matter. Such models, represented by analytical formulae and values of relevant parameters, are available in the literature[5,12], but packaging into a user-friendly code makes their use more efficient.

SHIELD11 is a semi-empirical shielding code designed specifically for use at high-energy electron facilities. It was developed by Nelson and Jenkins[10] at the Stanford Linear Accelerator Center. Its method it is analogous to the Moyer model initially developed for proton machines[24]. SHIELD11 assumes a very simple geometry: a shielding slab of thickness *d* is located at a distance *a* and angle α with respect to a cylindrical target of radius *r* and length *t*, as shown in Figure 9. Source terms for secondary species generated in the target and their attenuation in the shield and target itself are calculated using relatively simple analytical formulas derived from fits to experimental data and Monte-Carlo calculations. The model is based on a "thick target" assumption, requiring that the electromagnetic shower be fully developed in the target. This implies that the radius should be greater than 1 Moliere unit and longer than 10 radiation lengths in a given material, when accounting for neutron attenuation in the target is desired. Further restrictions on radius and length are imposed in terms of relaxation length for the direct-gamma component GamD (see below).

The source term in SHIELD11 is expressed in terms of dose equivalent rate [Sv/h] at one meter from target per kW of beam power. Only production of secondary photons and neutrons is taken into account, *i.e.* muons are not considered. The source term consists of the following five components:

- **GRN** (Giant Resonance Neutrons): neutrons generated in the core of the electromagnetic cascade by means of the giant-resonance production mechanism, with energies in the 0.1 MeV to 20 MeV range.
- **HEN** (High-Energy Neutrons): neutrons with energies above 100 MeV, resulting from hadronic cascade (see Silari & Stevenson[29]) initiated by high-energy photons above the photo-pion production threshold. This component is the most penetrating and dominates behind very thick shielding, but it manifests itself mostly by its byproduct, the lower-energy evaporation neutrons generated in outer layers of the shield.
- **MID** (Mid-Energy Neutrons): neutrons with energies between GRNs and HENs, including those generated by means of the pseudo-deuteron production mechanism
- **GamD** (Direct Gammas): Photons escaping from the electromagnetic cascade core in a thick target, with energies in the 0.1 MeV to 20 MeV range. This range corresponds to the broad minimum in the mass attenuation coefficient, called "Compton window".
- **GamI** (Indirect Gammas): Photons and charged particles resulting from interactions of HEN in the shield and escaping from the shield material

Yields and attenuation in the target material are calculated using the following parameters: atomic number Z, atomic mass A, mass attenuation factor μ, radiation length X_0 and Molière radius X_m . Parameters used to estimate attenuation in the shielding material are material density ρ, photon mass attenuation factor μ_s, and mean-free-path factors λ_i, i = 1,2,3, for the three neutron components (in g.cm^{-2}), as indicated in Figure 3. The total dose-equivalent, consisting of photon dose-equivalent H_p and neutron dose-equivalent H_n, are calculated at a point of interest behind the shield, situated at an angle θ from the target. Assuming that the radiation field exhibits a "$1/r^2$" variation with distance and attenuation is roughly exponential, the model used in SHIELD11 is summed up in the two equations below for H_p and H_n:

$$H_p\left[\frac{Sv.m^2}{h.kW}\right] = 0.225\times\left[\frac{\cos(\alpha-\theta)}{a+d}\right]^2 \times \left[\underbrace{\left(1.26\times10^6\, E\times e^{-(t-0.01X_0)\mu}\times e^{-\theta^{0.6}} + 230\times e^{-(r\mu-1.18)}\times e^{-\theta/72}\right)\times e^{-\frac{\mu_s d}{\cos(\alpha-\theta)}}}_{GamD} + \underbrace{\frac{0.27}{(1-0.72\cos\theta)^2}\, e^{-\frac{d\rho}{\lambda_1\cos(\alpha-\theta)}}}_{GamI}\right] \quad (9)$$

$$H_n\left[\frac{Sv.m^2}{h.kW}\right] = 0.225\times\left[\frac{\cos(\alpha-\theta)}{a+d}\right]^2 \times \left[\underbrace{\frac{13.7\times e^{-\frac{d\rho}{\lambda_1\cos(\alpha-\theta)}}}{A^{0.65}(1-0.72\cos\theta)^2}}_{HEN} + \underbrace{\frac{44.3\times e^{-\frac{d\rho}{\lambda_2\cos(\alpha-\theta)}}}{A^{0.37}(1-0.75\cos\theta)}}_{MID} + \underbrace{4.94Z^{0.66}e^{-\frac{d\rho}{\lambda_3\cos(\alpha-\theta)}}}_{GRN}\right] \quad (10)$$

The source term in SHIELD11 is not well suited for a thin target situation, such as when an electron beam hits a thin beam pipe wall under a glancing angle. Dinter and Tesch measured experimentally bremsstrahlung produced at various angles when a thin iron plate is struck at a glancing angle[30]. A variety of source terms for both thin and thick targets, including experimental data and MC calculations, are also listed in the shielding compendium by Fasso et al[12].

SKYHINE. This code combines source and shielding algorithms from SHIELD11 to provide the source term needed in equation (8). However, a $1/r$ dependency is assumed, instead of $1/r^2$. The code is mainly used to calculate the boundary dose, which is subject to a regulatory limit expressed in terms of dose equivalent per year. The required input is

therefore number of electrons lost per year. Furthermore, the user specifies the size of the roof through which neutrons escape, its thickness (if any), and the offset of the source from the roof. Lateral and longitudinal offsets can be specified as well. The code then calculates the corresponding solid angle, source terms for the three neutron components and their attenuation under the varying angles through the shielding in different directions. The source terms are modified to allow for contribution of scattered neutrons and generation of evaporation neutrons outside the target by the high-energy component. A single value of λ = 140 m is assumed for all three components, HEN, MID and GRN. Figure 7 demonstrates an excellent agreement with experimental data. The source term was specified using the actual beam power on target and calculations are compared to data in absolute value, without further adjustment.

MUON89. Simple recipes for muon attenuation can be found in Swanson[5] and Sullivan[31]. A more elaborate and less conservative algorithm is used in the MUON89 code[32]. In this analytical code the source term is obtained by integrating the muon pair production cross-section by the photon track-length distribution in the target. The latter is based on a analytical formula by Clément and Kessler[33]. The code allows to perform simple shielding calculations for thick targets and slab shields, where muon fluence at angles specified by the user is provided. MUON89 evolved from the GREEN code described by Nelson *et al*[34,35].

ACKNOWLEDGEMENTS

As a review article, this work is essentially a compilation of work done by others listed in references below, most prominently by Swanson, Nelson and Fasso *et al*. Partial support was provided by Department of Energy Contract DE-AC-03-76SF00515.

REFERENCES

1. Liu, J. C. and Vylet, V.: *Radiation Protection at Synchrotron Radiation Facilities,* these proceedings, SL009
2. Tigner, M and Chao, A. (Editors), *Handbook of Accelerator Physics and Engineering*, World Scientific, ISBN 9180238584 (1999).
3. Winick, H. (SLAC): private communication
4. Liu *et al*.: *Radiation Safety Systems for Accelerator Facilities*, these proceedings, SL014
5. Swanson, W. P.: *Radiological Safety Aspects of the Operation of Electron Accelerators*, International Atomic Energy Agency, Vienna, IAEA Report 188 (1979).
6. Freytag, E.: *Strahlenschutz an Hochenergiebeschleunigern*. G. Braun, Karlsruhe 1972
7. Nelson, W. R., Hirayama, H. and Rogers, D. W. O. *The EGS4 Code System*. Stanford Linear Accelerator Center, Stanford, CA 94087, SLAC-265 (1985).
8. Simulation performed using a web based EGS simulation tool designed by W. R. Nelson at Stanford Linear Accelerator Center. Access to the web site http://www2.slac.stanford.edu/vvc/egs/Default.htm at its development stage kindly granted to the authors by Dr. Nelson.
9. Particle Physics Booklet, American Institute of Physics, 1996
10. Nelson, W. R. and Jenkins, T. M., SHIELD11 code, Stanford Linear Accelerator Center, 1989
11. Mao, X. S, Fasso, A., Liu, J. C., Nelson, W. R. and Rokni, S.: *90º Bremsstrahlung Source Term Produced in Thick Targets by 50 MeV to 10 GeV Electrons*. SLAC-PUB-7722, January 2000.
12. Fassò, A., Goebel, K., Höfert, M., Ranft, J., and Stevenson, G. R: *Shielding against High-Energy Radiation.* Landolt-Börnstein, Numerical data and Functional Relationships in Science and Technology, New Series, Group I: Nuclear and Particle Physics, Volume 11, Springer-Verlag [Berlin] (1990).
13. Liu, J. C., Fasso, A., Mao, S., Nelson, W. R., Seefred, R. and Sit, R. *Environmental Impact from Accelerator Operation at SLAC*, Proceedings of 1999 Symposium on Environmental Monitoring Techniques, Kaohsiung, Taiwan, March 18-19, 1999. Also SLAC-PUB-8085 (1999).
14. Jenkins, T. M.: SKYSHINE computer code, Stanford Linear Accelerator Center, 1989
15. Lindenbaum, S. J.: *Shielding of high energy accelerators*, Annu. Rev. Nucl. Sci. 1, p.213 (1961)
16. Jenkins**,** T. M.:Accelerator Boundary Doses and Skyshine – A Review. Health Phys.27:251-257,1974
17. Nelson, W. R.: *The Shielding of Muons around High-Energy Electron Accelerators: Theory and Measurement*, Nucl. Instr. & Meth. **66** (1968), p. 293
18. Stevenson, G. R.: *Induced Activity in Accelerator Structures, Air and Water*, these proceedings, SL010
19. DeStaebler, H.C.: *Photon Induced Residual Activity*, SLAC-TN-63-092, Nov. 1963, Stanford Linear Accelerator Center

20. Patterson, H. W., and Thomas, R. H.: *Accelerator Health Physics*. Academic Press, ISBN 0-12-547150-5 (1973).
21. Fassò A., Silari M. and Ulrici L.: *Predicting Induced Radioactivity at High-Energy Electron Accelerators*, Journal of Nucl. Science and Technology, Suppl. **1**, 827(2000)
22. Rokni, S. H., Gwise, T., Liu, J. C. and Roessler, S.: *Induced Radioactivity of Materials by Stray Radiation Fields at an Electron Accelerator*, SLAC-Pub-8912, Stanford Linear Accelerator Center, July 2001. Submitted to Nucl. Instr. & Meth.
23. Fasso, A., Ferrari, A., Ranft J. and Sala, P. R. *The FLUKA Monte Carlo Code*, CERN, Geneva, Switzerland (2001).
24. Stevenson. G. R: *Shielding High-Energy Accelerators*,.these proceedings, SL007
25. Moritz, L.: *Radiation Protection at Low-Energy Proton Accelerators*, these proceedings, SL005
26. Silari, M.: *Specia Radiation Protection Aspects of Medical Accelerators,* these proceedings, SL018
27. Waters, L. S. (editor), *Monte Carlo N-Particle Transport Code System for Multiparticle and High Energy Applications, Version 2.2.3*, Los Alamos National Lab., Los Alamos, NM, MCNPX2.2.3 (2001).
28. Mokhov, N. V.: *The MARS code system user's Guide*, version 13(95), Fermilab Report FN-628, 1995, Fermi National Accelerator Laboratory
29. Silari, M. and Stevenson, G. R.: *Radiation Protection at High-Energy Proton Accelerators*, these proceedings, SL006
30. Dinter, H. and Tesch, K.: *Dose and Shielding Parameters of Electron and Photon Stray Radiation from a High-Energy Electron Beam*, Nucl. Instrum. Meth. **143**(1977), p.349.
31. Sullivan, A. H.: *A Guide to Radiation and Radioactivity Levels near High Energy Particle Accelerators*, Nuclear Technology Publishing, ISBN1 870965 18 3 (1992).
32. Nelson, W. R. and Namito, Y. , MUON89 computer code; Stanford Linear Accelerator Center, 1989
33. Clément, G. and Kessler, P.: *Electroproduction de muons de très haute énergie*, Nuovo Cimento **37** (1965) 876.
34. W. R. Nelson and K. R. Kase, *Muon Shielding Around High Energy Electron Accelerators. Part I: Theory*, Nucl. Instr. Meth. 120 (1974) 401.
35. W. R. Nelson, K. R. Kase, and G. K. Svensson: *Muon Shielding Around High Energy Electron Accelerators. Part II: Experimental Investigation*, Nucl. Instr. Meth. 120 (1974) 413.

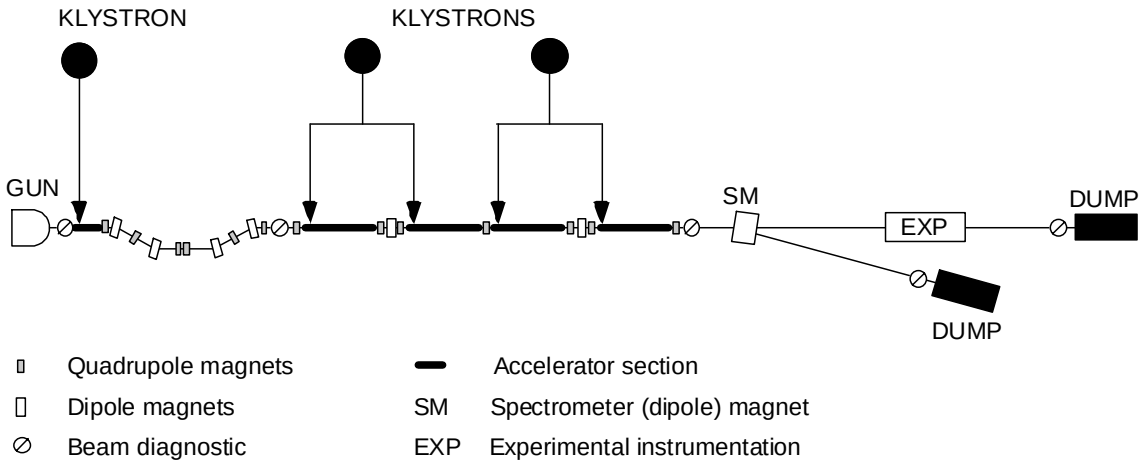

Figure 1: Example of typical accelerator components used in an electron linac. Arrows connecting klystron to accelerator sections represent RF waveguides. Klystrons are usually located outside the accelerator shielding (not shown here). Each symbol for dipole or quadrupole magnet represents one or more such devices.

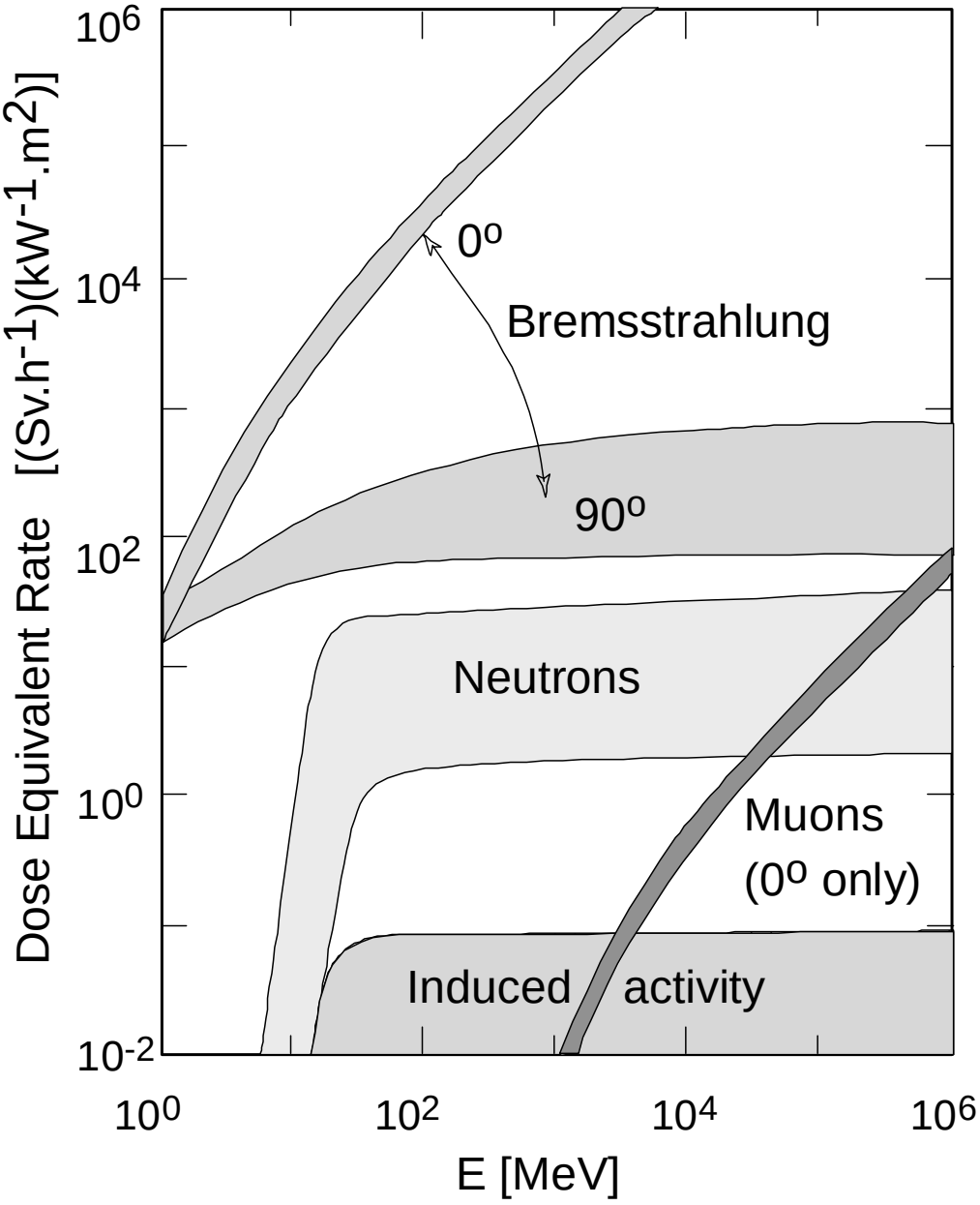

Figure 2: Dose equivalent rates per unit beam power to be expected from an electron beam striking beam line components, in the absence of shielding. The widths of the bands for different types of radiation indicate expected variations dependent on the type and thickness of target material. (Adapted from Swanson[(5)]).

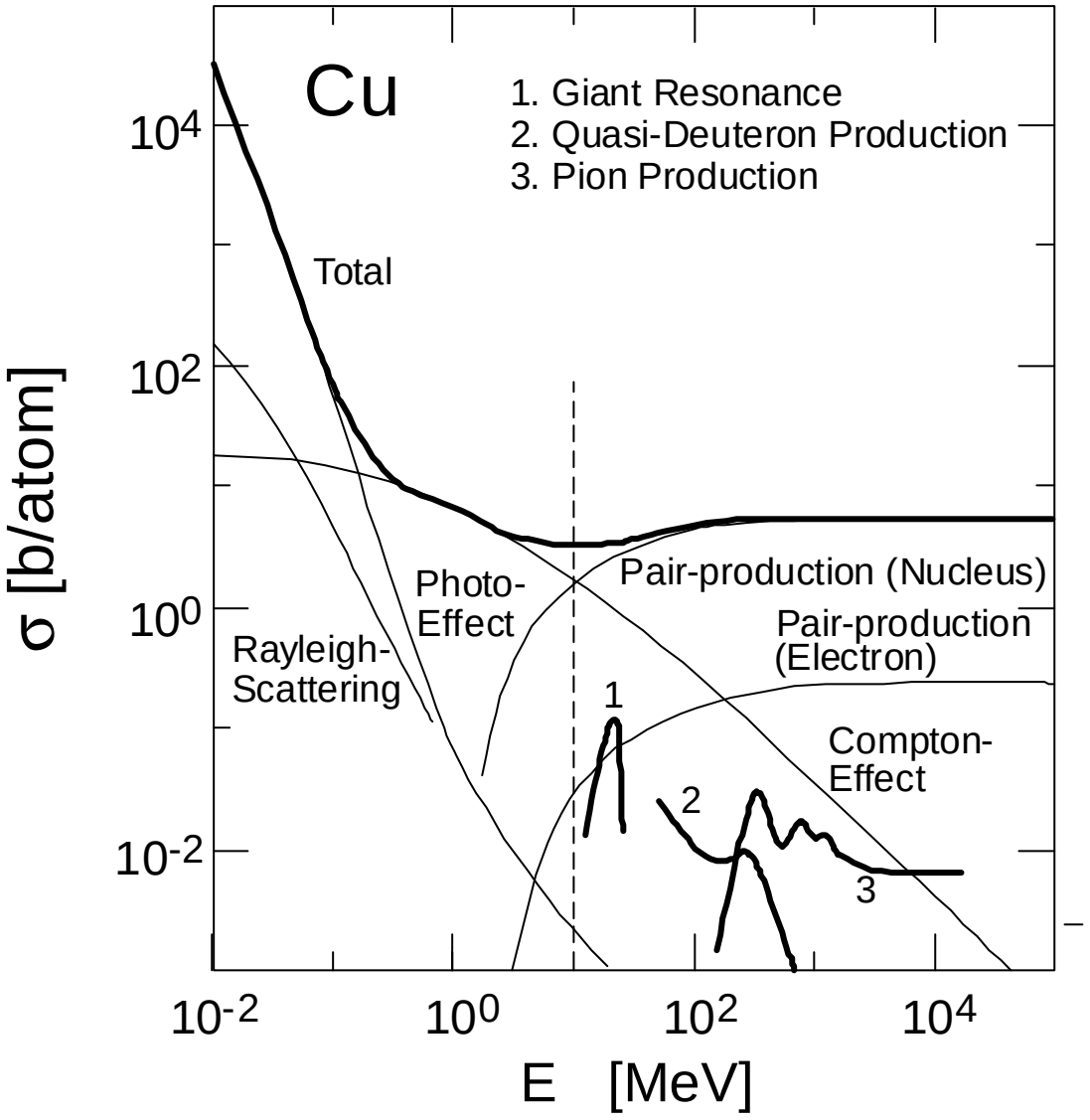

Figure 3: Cross-sections of major photon interactions in copper as function of energy. Processes labeled 1 through 3 are photonuclear interactions leading to production of neutrons. Maximum energies of bremsstrahlung photons generated around high-energy electron accelerators lie well above the dashed vertical line (adapted from Freytag[6]).

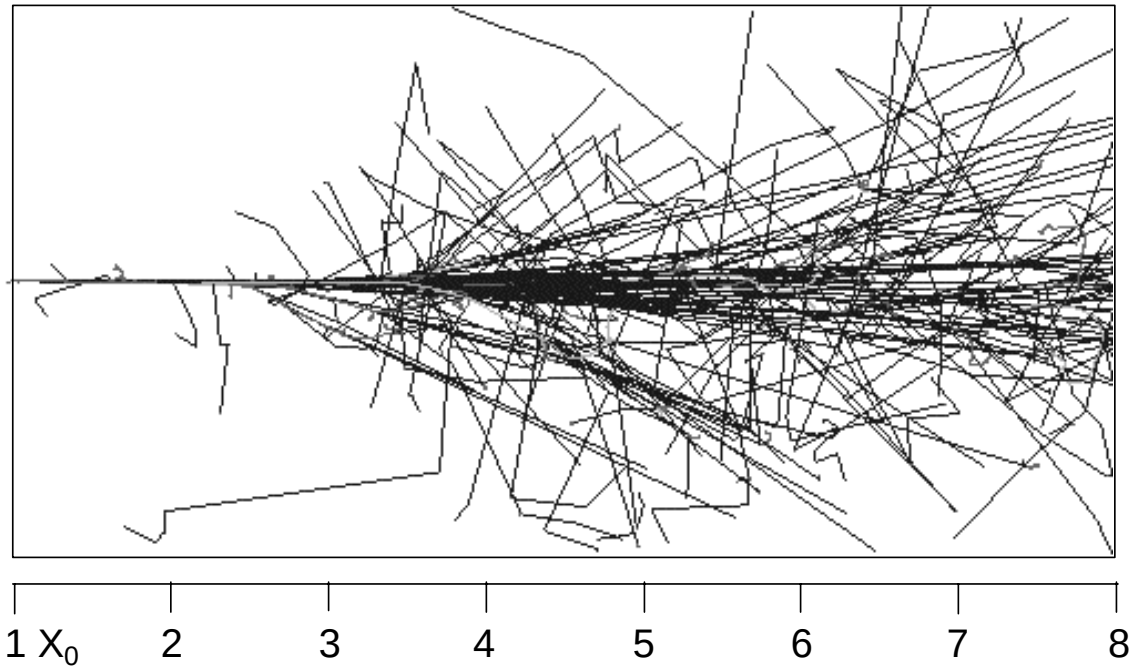

Figure 4: EGS4[7] simulation[8] of an electromagnetic shower resulting from a single 1 GeV electron within a cylindrical copper target with a radius of 2.5 cm and 10 cm long (this correspond to approximately 8 radiation lengths). Most of the visible tracks correspond to photons; electron and positron tracks are mostly very short and tortuous. The cutoff for all secondary particles was 0.1 MeV.

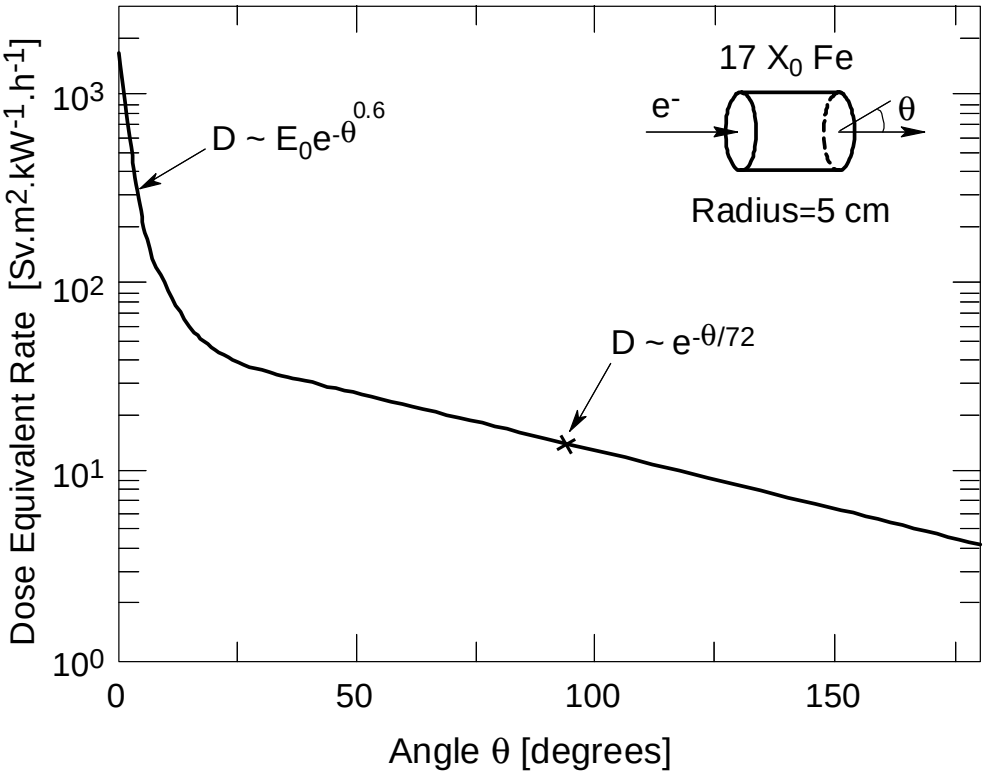

Figure 5: Photon dose equivalent rate from a thick target per unit electron beam power as a funcion of emission angle θ for a 1 GeV electron beam. This plot reflect the analytical model for narrow and wide-angle bremsstrahlung distributions implemented in the shielding code SHIELD11[(10)] by Nelson and Jenkins. The standard target in this code is an iron cylinder with a 5 cm radius and 17 radiation lengths long.

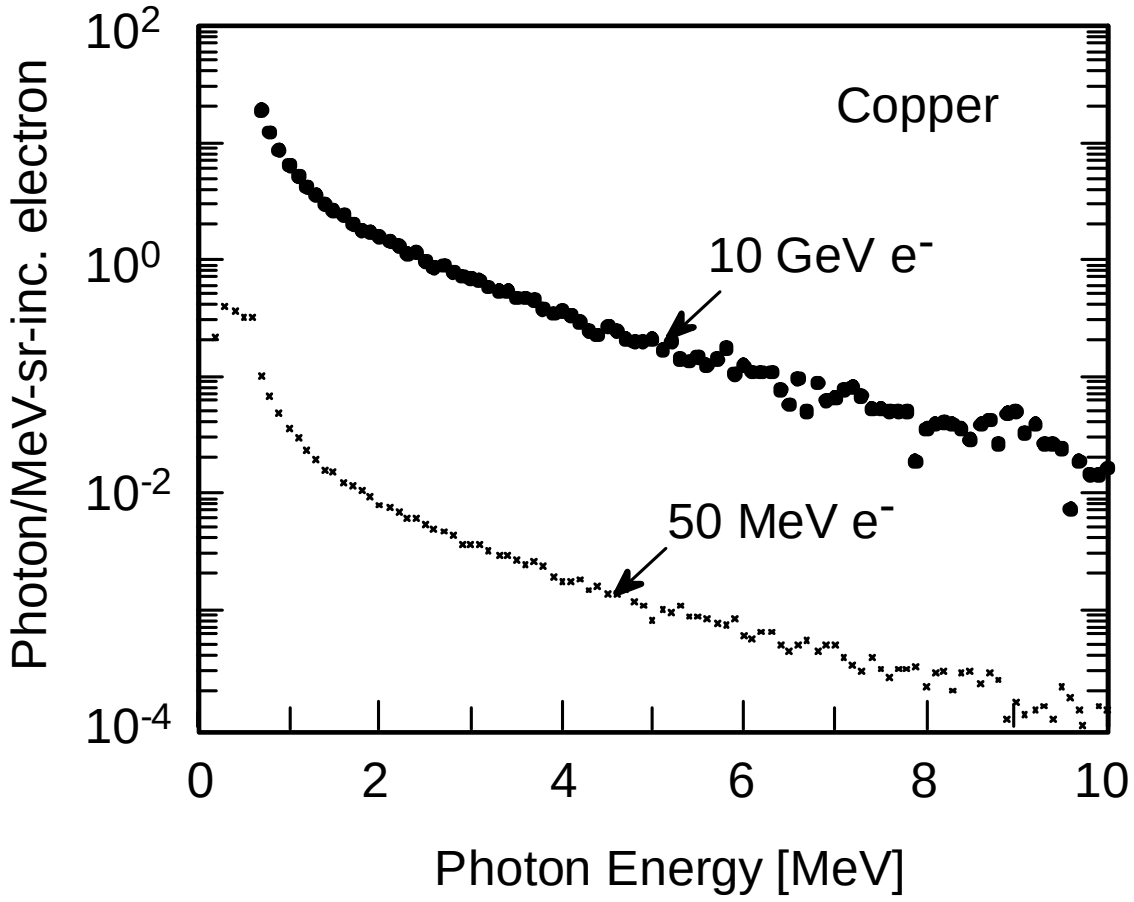

Figure 6: Photon spectra at 90 degrees from a thick copper target, 20 radiation lengths long and three Molière units in radius (adapted from Mao *et al*.[11], with kind permission of the authors).

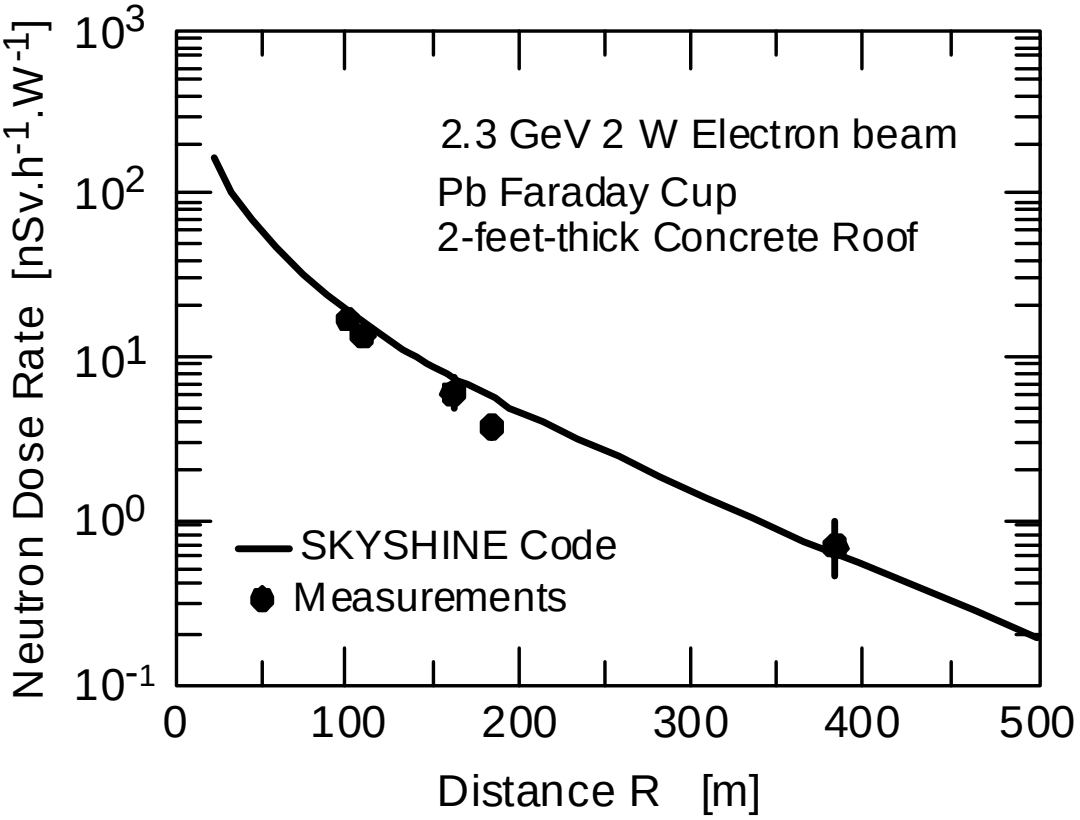

Figure 7: Measurement of skyshine from the SPEAR storage ring injection line compared with calculations using the SKYSHINE[14] analytic code (from Liu *et al*[13]).

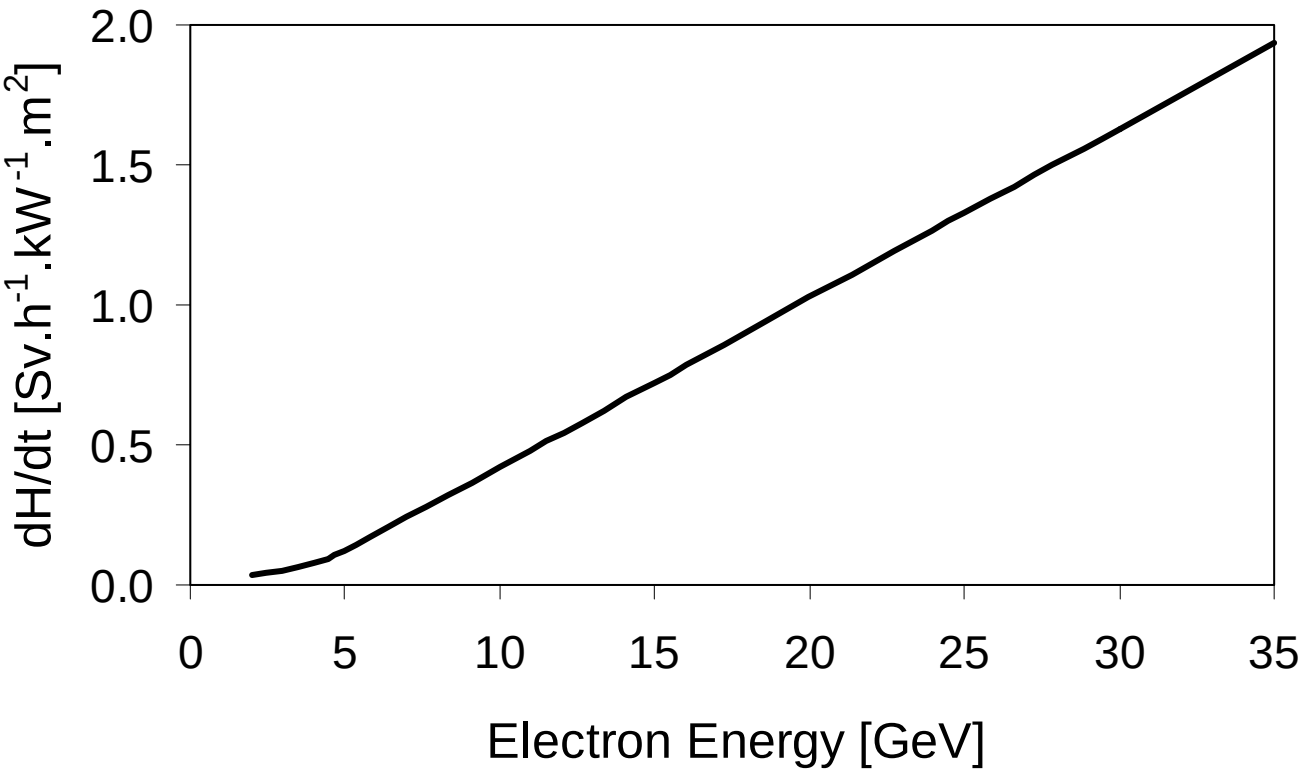

Figure 8: Muon source term in terms of dose equivalent rate per unit beam power at one meter at 0° from a thick iron target, as a function of electron beam energy (adapted from W. R. Nelson[17] with author's kind permission). The shape of the curve below 5 GeV and above 30 GeV is inferred by extrapolation.

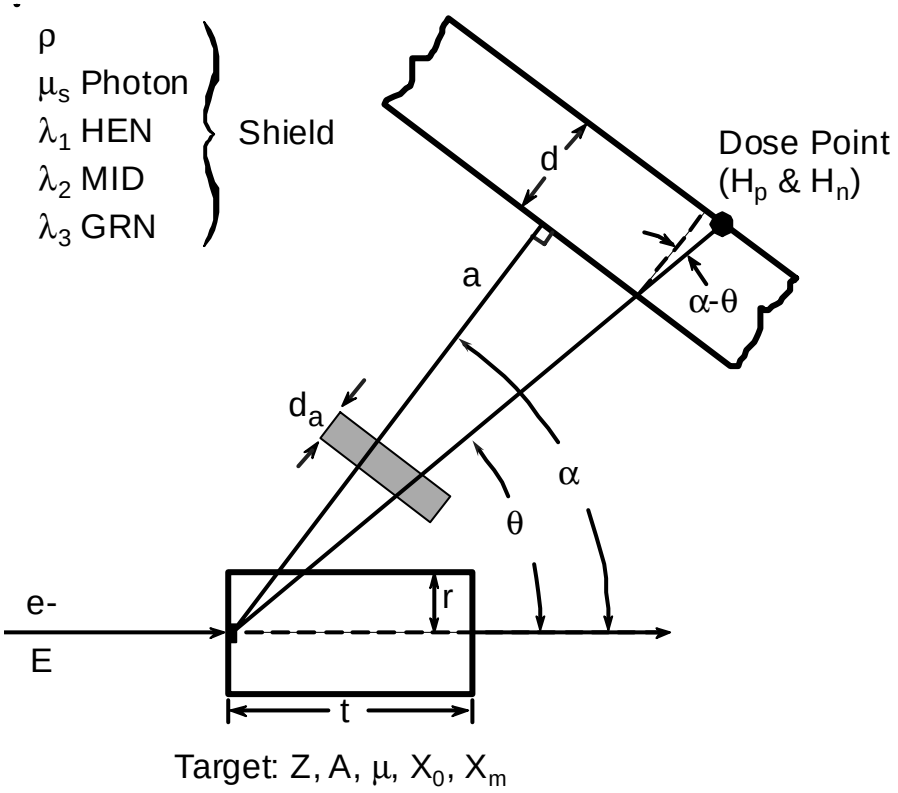

Figure 9: Geometry representation used in the SHIELD11 code: Photon and neutron dose equivalent is calculated at a point behind a primary slab shield. Additional "local" shielding of different material, situated between the target and the point of interest, can be taken into account. See text for the meaning parameters describing properties of target and shielding.